Nuclear Instruments and Methods in Physics Research B 365 (2015) 225–229

Contents lists available at ScienceDirect

Nuclear Instruments and Methods in Physics Research B

journal homepage: www.elsevier.com/locate/nimb

Distribution and evolution of thermal field formed by intense pulsed ion beam on thin metal target

Xiao Yu [a], Jie Shen [a], Miao Qu [b], Haowen Zhong [a], Jie Zhang [a], Yanyan Zhang [a], Sha Yan [b], Gaolong Zhang [a], Xiaofu Zhang [a], Xiaoyun Le [a,*]

[a] School of Physics and Nuclear Energy Engineering, Beihang University, Beijing 100191, PR China
[b] Institute of Heavy Ion Physics, Peking University, Beijing 100871, PR China

ARTICLE INFO

Article history:
Received 29 September 2014
Received in revised form 22 April 2015
Accepted 14 July 2015
Available online 25 July 2015

Keywords:
Intense pulsed ion beam (IPIB)
Thermal field
Thin metal target

ABSTRACT

Intense pulsed ion beam (IPIB) is characterized by short-pulsed high power density. With the strong thermal effect in the surface as the dominating feature, IPIB is an ideal technique for flash-heating surface processing of materials, especially for metals and alloys. Thus, the understanding of formation and evolution of thermal field induced by IPIB irradiation is of great significance to their application and diagnostic techniques. Due to the short pulsed duration and high energy flux of IPIB, the study in this field was so far mainly yield to numerical simulation. In this paper, with a combination of infrared image diagnostics, numerical analysis using Monte Carlo (MC) and finite element methods (FEM), the distribution and evolution of thermal field formed by IPIB produced by a magnetically insulated diode on a thin metal target was studied. The evolution of the thermal field and its effects on applications, such as the design of calorimeters was discussed reasonably.

1. Introduction

Intense pulsed ion beam (IPIB), is a technology originated from the 1960s for the purpose of inertial confinement fusion (ICF) ignition [1]. During the past three decades, as a means of flash heat source, IPIB has been extensively researched in the field of material science, especially the surface treatment of metals and alloys [2,3]. The advantage of IPIB lies in its feature that the high current density (in kA/cm^2 scale), short pulse duration (10–1000 ns) and short range of ions (typically in μm) induce a pulsed high power density in the surface region of the material. The surface region of several μm of depth can be melted, evaporated and re-solidified in the time scale from tens to hundreds of ns. Meanwhile, the induced thermal shock may affect deeper regions of the target up to 200 μm [4]. Surface layers with special properties, such as amorphous state, which is difficult to be produced using conventional methods, can be prepared with IPIB [2].

As the material response of IPIB is largely dominated by the thermal effects induced from its high power density, the research of IPIB energy deposition and thermal field evolution is of great significance to the science and engineering exploration. In previous research, the study of IPIB induced thermal field distribution and evolution was mainly carried out by numerical simulations as the direct observation of the dynamical processes on the surface is quite challenging [5]. These numerical researches, although largely deepened our understanding to the IPIB thermal response, still need further development and certification via combination with state-of-art diagnostic techniques. Also, the model scale for IPIB research also calls for expansion. In the past two decades, the numerical research mainly focused on the evolution of thermal field in the time scale of hundreds of nanoseconds and spatial scale of several μm, for the purpose of analysis of extremely high energy flux irradiation effects [5]. However, for the design of diagnostic instruments with energy deposition methods such as calorimeter and thin-plate infrared imaging diagnostics, it is of paramount importance to estimate the establishing time of thermal field in the target in order to select optimized parameters (sampling time, frequency, etc.) and for error evaluation. Moreover, in previous simulation studies there exit some modeling flaws such as using a wrong energy deposition model (e.g., using Beer's law for ion energy loss [6]); as well, there are some simulation parameters taken by subjective approximation instead of experimental diagnostics (e.g., taking some evolution and distribution behavior as Gaussian [7]). In this model, we established an IPIB energy deposition and thermal response model based on the latest results of IPIB diagnostic techniques, and then a multi-step one-dimensional temperature model with radiation power loss was built to analyze

* Corresponding author. Tel.: +86 010 82325842.
E-mail address: xyle@buaa.edu.cn (X. Le).

http://dx.doi.org/10.1016/j.nimb.2015.07.061
0168-583X/

the long-time scale temperature field spatial revolution and its effects on relative applications.

2. Model and method

When IPIB bombard a material, the energy of the ions is transferred to the target electrons and ions, i.e. the electron and nuclear stopping of incident ions, respectively. As the stopping process of ions (in 10^{-13} s scale) is much shorter than the duration of IPIB (in 10^{-8} s scale or more), so we can take that, the time spent on ion stopping is negligible compared with the IPIB pulsed energy deposition process in the target. In general, the modeling of temperature field evolution generated by IPIB can be divided into two problems: the first is the power density distribution and evolution in the target, i.e., mathematically, the source term of the model; the other is to depict the response of the target to the source term.

2.1. IPIB power density distribution in the target

Typically, IPIBs are generated by magnetically insulated diode (MID) with dense plasma emission on the anode surface in order to achieve high particle flux. In previous research, it was taken that the energy of the ions is defined by the working voltage of MID and the current density of the beam controls the number of ions bombarding the target. Thus, the power flux of IPIB was often calculated by taking the product of MID working voltage and beam current density [7]. However, there are drawbacks in this approximation: the MID working voltage is not equal to the accelerating voltage applied on the ions because the emission of IPIB only starts when the voltage of MID exceeds certain value. Also, there exists a time delay between the MID working voltage pulse and beam current density pulse which is difficult to determine, yet obvious changes in the power flux may be caused as it changes. Now we take another point of view: If the cross-sectional energy density distribution of the beam is known (e.g., with means such as calorimeter matrix or thermal imaging diagnostics), in order to completely characterize the power density distribution in the target, it is necessary to take the followings into account:

- The spatial distribution of energy in the target along the depth, which is defined by the ion type, energy and the characteristics of the target materials. Here we use relative distribution function of beam energy vs. the depth $d(x)$ determined by the stopping power of ions dE/dx which can be calculated by Monte Carlo method such as SRIM. The IPIB particle energy and spectrum features can be measured by Thompson parabola spectrometer and time-of-flight (TOF) method [8].
- The temporal evolution of energy deposition in the target, we take the current density evolution function $f(t)$ for description. Here we take the curve acquired by the Faraday cup which is used to detect the IPIB current density as IPIB power evolution function. Unlike usually taken as Gaussian, in most of our experimental measurements, $f(t)$ is characterized by a relatively longer falling time than rising time which is shown in Fig. 1.

Take $d(x)$ and $f(t)$ as normalized function, then the power density distribution function can be expressed as follows:

$$P(x,t) = k \cdot d(x) \cdot f(t) \tag{1}$$

where k is the cross-sectional beam energy density on the target surface with dimension energy per unit area. In one-dimensional case, k is taken as constant; in three-dimensional problem, k can be expressed as $k(x, y)$ and can be measured by infrared imaging methods [9].

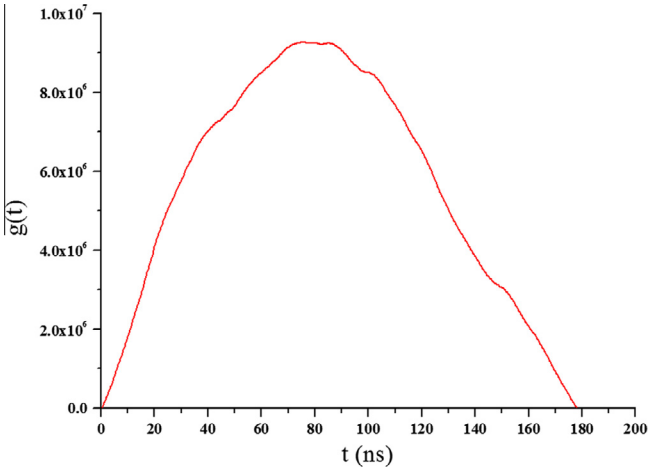

Fig. 1. Temporal evolution function of IPIB power.

2.2. Heat transfer model

In general, the heat conduction equation in the target can be described by Fourier Law and energy conservation law as:

$$\rho(T)C(T)\frac{\partial T}{\partial t} = \lambda(T)\frac{\partial^2 T}{\partial x^2} + P - E \tag{2}$$

$$E = L\delta(T(x,t) - T_m) \tag{3}$$

where $\rho(T)$ is the density of the material, $C(T)$ is the specific heat, $\lambda(T)$ is the thermal conductivity and P is the source term, i.e. the IPIB power density distribution function given above. In this work, $\rho(T)$, $C(T)$ and $\lambda(T)$ are temperature-dependent functions taken from Material Property Database (MPDB) of JAHM Software, Inc. E denotes the term of fusion latent heat. L is the latent heat of fusion, T_m is the melting temperature. The initial condition is $T(x, 0) = T_0$ (T_0 = 298 K). As the air pressure in the vacuum chamber is lower than 10^{-2} Pa, convective heat transfer can thus not be taken into account. In order to estimate the energy loss by surface-to-ambient radiation, Stefan–Boltzmann boundary condition was adopted:

$$j = \varepsilon\sigma(T^4 - T_0^4) \tag{4}$$

in which j is the surface-to-ambient radiation heat flux, σ is the Stefan–Boltzmann constant, ε is the emissivity. In this work, for a cleaned surface of metal we take $\varepsilon = 0.3$. The equation is solved by finite element method (FEM) program Comsol Multiphysics [10].

3. Results and discussion

The simulation was carried out with stainless steel and copper of different thickness. The normalized energy distribution function $d(x)$ is calculated from the results of Monte Carlo code SRIM. The ion type and energy spectrum of the beam are taken from Ref. [8]. The normalized power evolution function $f(t)$ is calculated from the parameters acquired with the accelerator BIPPAB-450 [11,12] with a Faraday cup with biased magnetic field in order to cut off the neutralizing electrons in the beam. The beam energy density obtained by one-dimensional simulations is 1 J/cm^2.

3.1. IPIB power deposition

As shown in Fig. 2, the energy loss function vs. depth is dominated largely by the ion energy. When taking into account the low energy ions component, the energy loss tends to have the maximum value on the target surface; this obviously differs from the

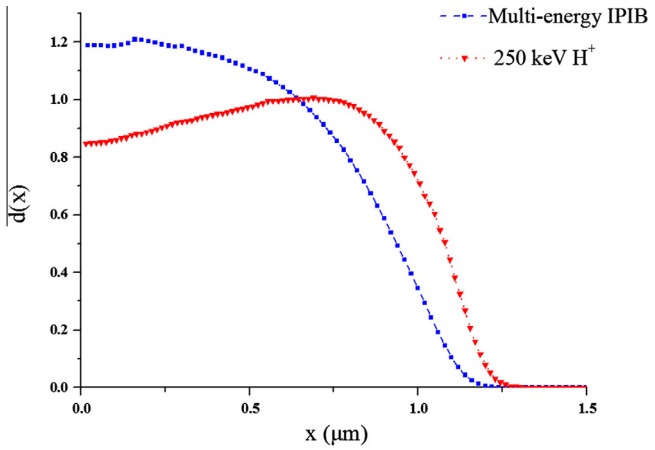

Fig. 2. Relative distribution function of beam energy vs. the depth x of 250 keV proton beam and multi-energetic beam in 304 stainless steel.

energy loss profile of a mono-energetic proton beam characterized by the Bragg peak. Also, as there does not exist the small portion of high energy ions like in Gaussian distribution, the tail of $d(x)$ is much smaller. During the period with large power flux, the shape of energy loss function $d(x)$ greatly defines the spatial distribution of the temperature field as that the injected power is much higher than that transferred by conduction. This may strongly affect the material responses for IPIB bombardments, e.g., for the beam which made up of monoenergetic protons, the temperature rising in the subsurface layer may be faster than that on the surface, this may cause prior evaporation and ejection from the deeper region in the target and surface features such as volcano may be caused. In our study, as the energy loss of the beam has the maximum value on the surface, the highest temperature appears on the surface. The melting and evaporation correspondingly first take place on the surface region, and as a result, surface morphologies with fierce convection and ejection of molten surface, such as volcano surfaces, may not be generated.

3.2. Temperature field evolution

Fig. 3 shows the temperature evolution of 304 stainless steel within the first microsecond after IPIB bombard on target. As the

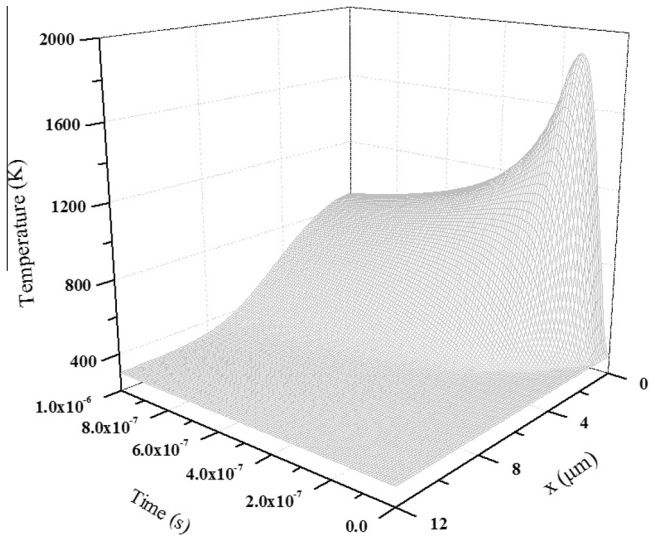

Fig. 3. Temperature evolution with time and depth x in 304 stainless steel in the first microsecond after IPIB irradiation.

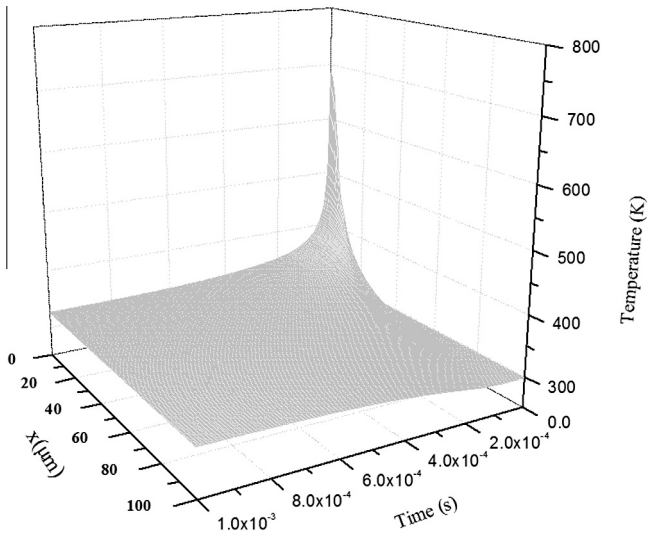

Fig. 4. Temperature evolution with time and depth x in 304 stainless steel in the first millisecond after IPIB irradiation.

irradiated beam power density increases and decreases sharply, the temperature of the target within the ion range varies sharply at the same period. As the power injection is much more than that is conducted, the temperature change in this stage is mainly located in the depth of about several times of the ion range. For the region with depth of more than 12 μm in the target, the temperature remains unchanged during the first microsecond. The temperature evolution within the region of the ion range shows a strong correlation with the power evolution. When the beam stops, the heat conducting to the deeper region in the target gets the advantage and results in a falling of the temperature field near the front surface. These results are similar to previous research with different ion species and energy [5–7].

Fig. 4 shows the temperature evolution of stainless steel in the succeeding 1 ms in a 100 μm stainless steel target. As the heat in the target is conducted to the deeper region of the target, the temperature near the surface falls gradually. Meanwhile, in the deeper region close to the rear surface of the target where the heat is transferred to, the temperature rises, but in a slow trend. At the time of 1 ms, the temperature difference between the front and the rear surface of the target is within 0.1 K. We can take it that the target has been uniformly heated by the beam. This implies that, for applications like calorimeter and infrared imaging diagnostics, this time is the minimum time delay between the beam emission and data capture. When the thickness of the target increases, the time of temperature field establishment t_e (here we define this as the time spent for the temperature difference between the front and rare surface to be less than 0.02 K) was also extended. For different material t_e may varies obviously considering the difference in the thermal diffusivity. For the experimental test of the present work we took materials with relatively high (copper) and low (stainless steel) thermal diffusivity, where t_e varies by two orders of magnitude. For each material we used t_e and the target thickness d, which ranging from 50 to 1 mm, generally have a quadratic function relationship (see Fig. 5). For different materials, t_e for a certain d can be estimated with the principles above, which implies that, for most heat deposition diagnostics for IPIB with heat sink plate (usually with relatively large heat conductivity coefficient and high melting point material such as tungsten and graphite) with thickness typically of 1–2 mm, the time delay between IPIB irradiation and data sampling is within 0.1 s.

As for the effect of radiative energy loss, we took a longer time scale of 10 s and recorded the power loss j due to

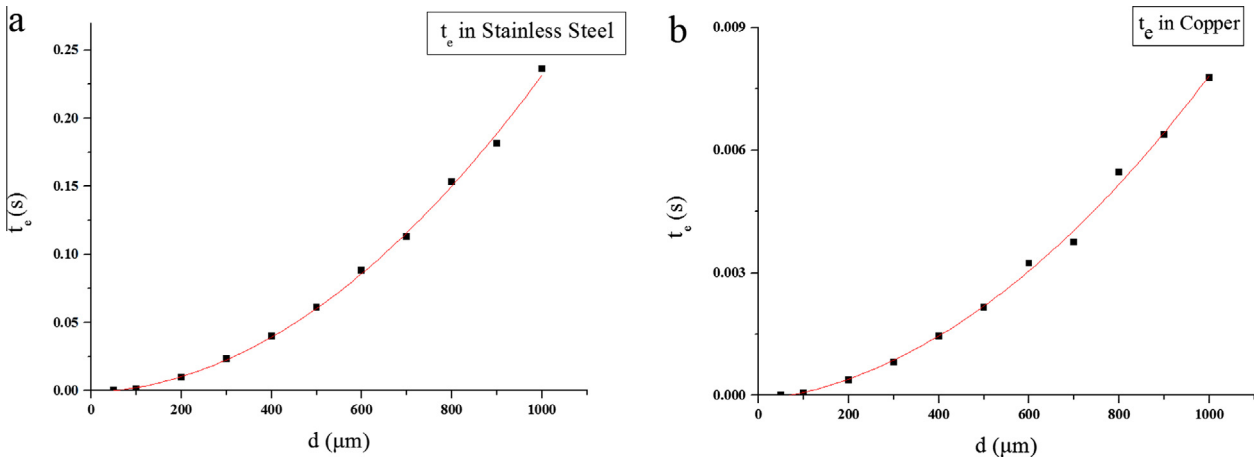

Fig. 5. Thermal field establishing time t_e vs. thickness of the target in 304 stainless steel (a) and copper (b).

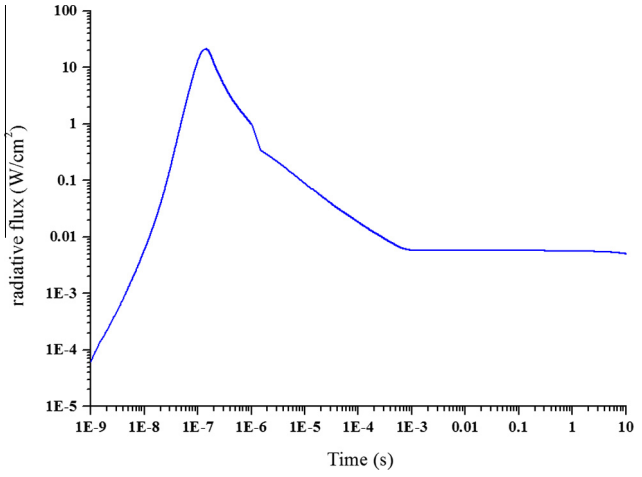

Fig. 6. Surface-to-ambient radiative heat loss of 304 stainless steel after IPIB irradiation.

surface-to-ambient radiation. As shown in Fig. 6, j is considerately large as the surface temperature increases sharply during IPIB irradiation. However, due to the short pulse duration, the total radiation energy loss is quite low (4.23E−6 J/cm^2). In the next ms, as the temperature falls rapidly on the surface, j decreased quickly but the radiation loss increase (1.60E−5 J/cm^2) as the period is longer. In the time scale of 1 ms to 1 s, the radiation losses increase to 5.67E−3 J/cm^2 and further, to 5.35E−2 J/cm^2 at 10 s. For a 100 μm target, this will cause an energy loss of 5.35%, corresponding to an error of the same percentage for the infrared imaging diagnostics.

However, in real situation, considering the surface distribution of energy density, there may be lateral heat conduction which may change the temperature distribution and thus cause a difference of energy losses comparing with the situation taking merely the radiation loss into account. As a result of lateral heat transfer, the temperature drop at the high temperature region on the surface of the target may be faster than merely taking radiative loss as that corresponds to the one-dimensional case. For the period within t_e, as the size of the beam (in cm) is much larger than the range of incident ions (~1 μm) the temperature gradient along the depth is much larger than the one along the target surface, thus the lateral heat transfer during t_e is negligible. After t_e, as the

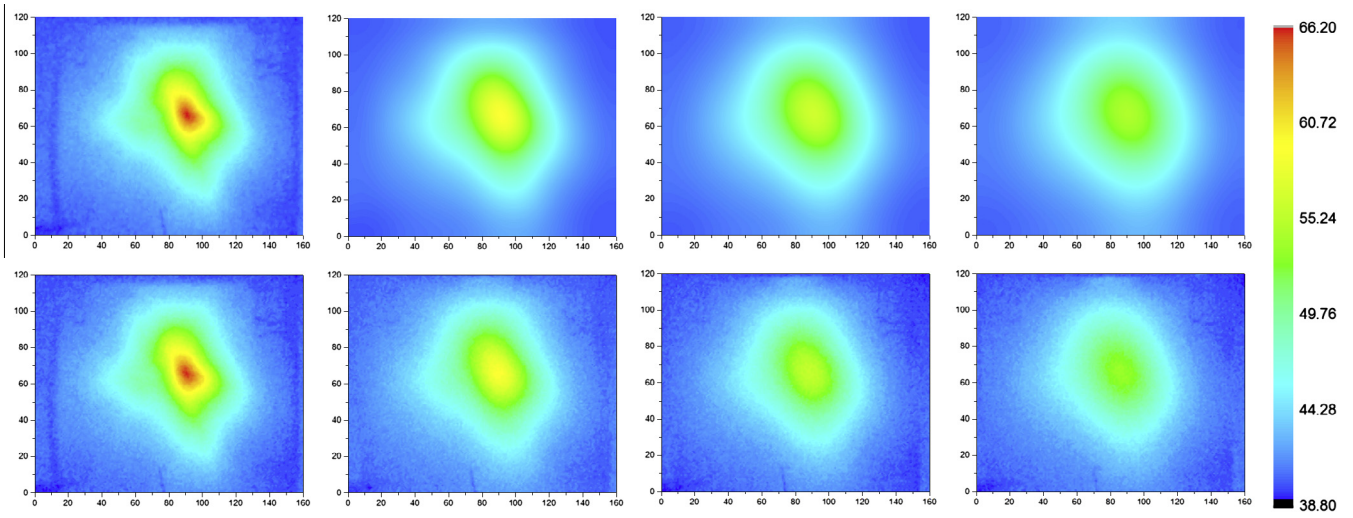

Fig. 7. Experimental (below) and calculated (above) thermal prints evolution of IPIB on 120 × 160 mm^2 100 μm stainless steel, time points (from left to right): initial, 5, 10, 15 s.

temperature difference is quite small between the front and rear surfaces of the target, the main heat conduction is the lateral one. Under such circumstances, two-dimensional thin-shell conduction model, regardless of the target thickness, can well describe the thermal pattern distribution and its evolution on a thin target with large width-depth ratio. From Fig. 7 we can see that in the time within 15 s, the lateral thermal conduction may lead to obvious thermal field diffusion, and thus the temperature field distribution becomes more even and its symmetry will get better. For the thin metal plate infrared diagnostics, an error can be caused due to this reason.

4. Conclusions

A new model is built to characterize the power density distribution of IPIB in the target. The model, combined with IPIB diagnostic methods, can be used to calculate the temperature field distribution and evolution, and can be extended into 2 and 3-dimensional case. This work can provide some theoretical reference to the optimization of parameters for the calorimetric diagnostic methods of IPIB such as calorimeters and infrared imaging diagnostics. Under the research conditions of this work, the following conclusions are acquired:

(1) The energy deposition profile is largely dominated by the energy spectrum of the ions. The low energy ions contribute to a larger deposition portion near the surface. As a result, the melting and evaporation of the target tend to begin at the surface of the target.
(2) IPIB can lead to sharp rise and fall in the target in the region of several times of the ion range. For thin metallic targets of a hundred microns, the time spent on the thermal equilibrium of the two surfaces is within the millisecond order, and for a given material, the time and the target thickness, within millimeters, are generally in a quadratic relationship.
(3) The radiative energy loss during the thermal equilibrium establishing process is very low and can be neglected for diagnostics. After the thermal equilibrium between the front and the rare surfaces of the target is built, the thermal field on a thin target (with thickness of tens to hundreds of microns) can be described by the thin shell thermal conduction model. In this stage, the lateral heat conduction becomes the dominate effect and it may lead to error in heat deposit diagnostics.

Acknowledgments

This work is supported by National Natural Science Foundation of China by Contract No. 11175012. We appreciate Doctor G.E. Remnev, Doctor A.I. Pushkarev, Miss Yu.I. Isakova and Mr I.P. Khailov of Tomsk Polytechnic University for their support in improving the experimental works in this paper.

References

[1] S. Humphries Jr, Intense pulsed ion beams for fusion applications, Nucl. Fusion 20 (12) (1980) 1549.
[2] G.E. Remnev, I.F. Isakov, M.S. Opekounov, et al., High intensity pulsed ion beam sources and their industrial applications, Surf. Coat. Technol. 114 (2) (1999) 206–212.
[3] T.J. Renk, P.P. Provencio, S.V. Prasad, et al., Materials modification using intense ion beams, Proc. IEEE 92 (7) (2004) 1057–1081.
[4] X. Le, S. Yan, Z. Liu, et al., Detection of shocks generated by intense pulsed ion beam irradiation, Surf. Coat. Technol. 201 (9) (2007) 4991–4994.
[5] L. Xiaoyun, Y. Sha, Z. Weijiang, et al., Computer simulation of thermal–mechanical effects of high intensity pulsed ion beams on a metal surface, Surf. Coat. Technol. 128 (2000) 381–386.
[6] L. Li, X. Xiang, Y. Lei, et al., A new method to investigate the intense pulsed ion beam ablation of silica, Nucl. Instr. Meth. Phys. Res. Sect. B 312 (2013) 131–136.
[7] D. Wu, Y. Gong, J.Y. Liu, et al., Model of intense pulsed ion beam and simulation study of energy deposited on target, Surf. Coat. Technol. 201 (15) (2007) 6573–6575.
[8] Yu I. Isakova , A.I. Pushkarev, V.A. Tarbokov, Measurement of composition and energy spectrum of pulsed ion beam with high-precision time-of-flight method, Proceedings of Tomsk Polytechnic University, 2010, 316(2) (Russian edition).
[9] Y. Isakova, Infrared imaging diagnostics for parameters of powerful ion beams formed by a diode in a double-pulse mode, in: A. Ads (Ed.), 2011 IEEE Pulsed Power Conference (PPC), IEEE, 2011, pp. 334–340.
[10] A.B. Comsol, COMSOL multiphysics user's guide, Version: September, 2005.
[11] G.E. Remnev, E.G. Furman, A.I. Pushkarev, et al., A high-current pulsed accelerator with a matching transformer, Instr. Exp. Tech. 47 (3) (2004) 394–398.
[12] É.G. Furman, A.V. Stepanov, N.Z. Furman, Ionic diode, Tech. Phys. 52 (5) (2007) 621–630.